Korea-Australia Rheology Journal (2023) 35:157–168
https://doi.org/10.1007/s13367-023-00063-0

ORIGINAL ARTICLE

Effect of electro-osmosis on lubrication of fresh cement paste-based material in contact with a metal wall

Viet Hai Hoang[1] · Tu Anh Do[1] · Anh Tuan Tran[1] · Christophe Lanos[2] · Yannick Mélinge[3]

Received: 19 December 2022 / Revised: 7 June 2023 / Accepted: 14 June 2023 / Published online: 3 July 2023

Abstract
This paper presents an experimental investigation of the effect of electro-osmosis on lubricating the interface between the cement paste-based material and metal wall. A new experimental apparatus was developed and set up in this study. Two scales of cement paste-based materials were used and tested: cement paste and mortar. Tests performed were as follows: (i) range of potential difference varies from 5 to 30 V; (ii) range of metallic plate slope varies from 7° to 15°. The pre-movement time was reduced and the sample velocity was increased by increasing the potential difference and the slope. The rheological properties of two mixtures were determined to identify the characteristics of the fluid film at the interface that plays an important role in lubricating the sample. The permeability coefficient for managing the contact lubrication was also determined in this study.

Keywords Electro-osmosis · Cement paste-based material · Rheology · Electro-tribometer

1 Introduction

Extrusion is a common manufacturing process used in many industrial sectors. In civil engineering, this process is widely used for panel, pipe, and brick fabrications at a highly productive rate. With the development of 3D-concrete printing, the extrusion of cement-based materials has recently gained close interest [1–3]. Applications of extrusion in the concrete industry consist of ram extrusion (Fig. 1a), which is often used in laboratories to study extrusion flows, describe the rheological behavior, and assess the extrudability of various materials, and screw extrusion (Fig. 1b), which is the most common extrusion technique, in which the material is continuously fed into the extruder barrel. Screw extruders are also used at the laboratory scale to test extrudable materials and optimize mixtures.

Due to its relatively infrequent use in civil engineering, the extrusion of cement-based materials has not been studied intensively. Cement-based materials behave like viscoplastic materials and exhibit a non-Newtonian behavior with respect to yield stress. These materials are formulated from polydisperse nature, sensitive to water drainage, and are consolidated during extrusion. Interaction between the extrudable material and extruder barrel dissipates energy. The tribological behavior of fresh mortar against a metal plate with different textures has been studied by Mélinge et al. [5]. Several authors have studied the optimal mixture ingredients and extrudability [6], which show a dominant plastic rheological behavior and do not have granular interactions.

Another issue in making an extrudable cement-based material is reducing partial friction between it and the extruder barrel using the principle of electro-osmosis. Perrot et al. and Toutou et al. [1, 6] used vibration to make a more extrudable material. Djelal et al. [7] has used the principle of electro-osmosis to lubricate a wall surface subjected to friction caused by the extrusion of the clay paste. Goudjil [8, 9] and Vanhove [10] used this process in formwork removal.

A process based on the principle of electro-osmosis was developed that allows water migration into concrete using double-layer properties of fine concrete particles. The principle is the application of an electric potential to the concrete

✉ Viet Hai Hoang
hoangviethai@utc.edu.vn

[1] Faculty of Civil Engineering, University of Transport and Communications, 3 Cau Giay, Lang Thuong, Dong Da, Hanoi, Vietnam

[2] Laboratoire de Génie Civil et Génie Mécanique, UNIR, Université de Rennes, 3 rue du Clos Courtel, 35704 Rennes, France

[3] Laboratoire de Recherche des Monuments Historiques (LRMH – CRC UAR 3224 CNRS), 29 Rue de Paris, 77420 Champs sur Marne, France

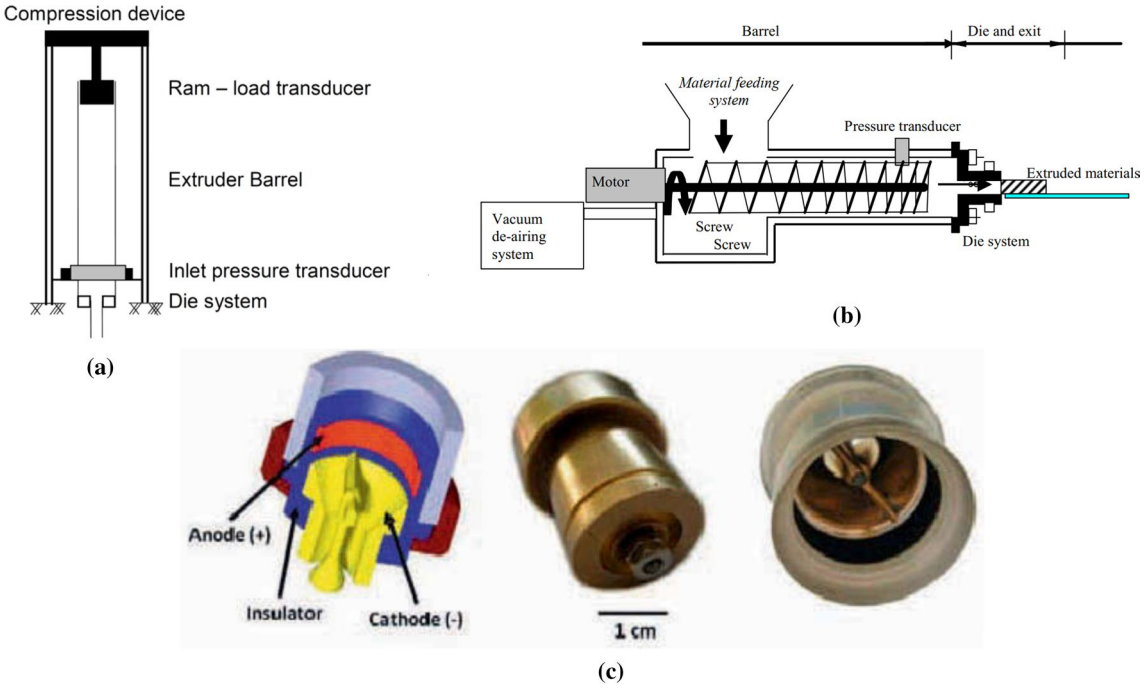

Fig. 1 **a** Schematic of ram extrusion and **b** of screw extrusion process [3] **c** Setup of electro-osmosis applied in screw extrusion [4]

by attracting the cations toward the cathode and the anions toward the anode. When the cations migrate toward the cathode, interstitial water is carried along with them. This generates a movement of water toward the cathode. This phenomenon was described by Casagrande et al. [11], who applied this principle to displacing water in clay. It was also applied to soils by Mitchell et al. [12] and Cambefort et al. [13]. Recently, the principle of electro-osmosis has been set up in a screw extrusion [4]. The tests indicated that the extrusion force can be reduced by 22.3% when a voltage 20 V was applied (Fig. 1c).

In this paper, an electro-tribometer based on the inclined plate technique has been developed to examine the lubrication effect induced by the principle of electro-osmosis. In this way, normal and shear stresses are imposed by the weight of each sample and plan inclination. The effect of electro-osmosis on lubricating the cement-based material samples in contact with the wall surface was confirmed [8, 9, 14]. The objective of this study is to evaluate the effect of electro-osmosis (potential difference and slope angle) on the displacement shape of the sample. By observing the steady-state regime of sample movements, we suppose that the effect of electro-osmosis changes the rheological properties of the film fluid at the wall surface and the sample. Moreover, the film thickness and solid volume fraction vary with the electrical potential difference. Finally, this process can be controlled via the electro-osmotic permeability coefficient.

Table 1 Mixing composition optimizes for ram extrusion

Items	Weight ratio constituent/powder for cement paste	Weight ratio constituent/powder for the mortar
Powder	1	1
fine sand (0/0.630 mm)	–	0.8
Water	0.22	0.25
Plasticizer Sika 22S	0.0075	0.0075
Powder (weight ratio): 70% cement, 20% volcanic rock finely crushed, 5% silica fume, 5% amorphous crushed quartz		

2 Materials

The used cement paste and mortar are equivalent to proposed one by Toutou [6], and the mortar preparation protocol is also equivalent. The mixing composition was optimized in recent research as shown in Table 1.

3 Experimental devices and test protocols

3.1 Electro-tribometer

To study the effect of electric polarization technique on lubrication at the contact between the cement paste sample and the metal plate, an electro-tribometer was developed and validated in the laboratory [14]. It is composed of an inclined metallic plate on which a rectangular sample is placed as illustrated in Fig. 3. The roughness of the steel wall was measured and controlled. The slope of the steel plate was also checked and set up before testing.

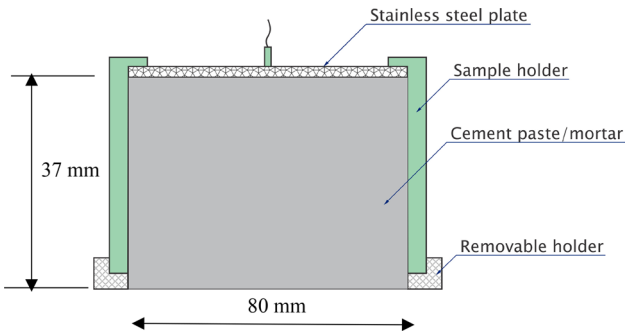

Fig. 2 Schematic of the sample holder

The sample holder (Fig. 2) allows the realization of a parallelepiped sample of 120 mm in length, 80 mm in width, and 37 mm in height. The bottom of the holder consists of a removable stainless 1-mm-thick steel plate which represents the second electrode. Finally, the sample holder is equipped with a removable holder so that only the sample is in contact with the wall surface (Fig. 2).

After the cement-based material sample was put in the sample holder, the removable holder was removed. The top of the sample holder was made of stainless steel which constitutes the anode (Fig. 3). The sample was weighed and placed on the inclined plate which was connected to the cathode. After the direct current (DC) power was activated, the sample starts to move. For one test, the imposed potential is kept constant, and the sample displacement is measured using a magnetostrictive sensor.

Depending on the potential difference and the slope angle, the sample movement will continue or stop. In case the sample movement continues, the sample average velocity will be determined from the steady-state regime of sample movements (Fig. 4). After testing, the sample is then weighed for the determination of mass loss. The test plan including changing the slope and potential difference will be conducted with one mixture.

The constant resistance R_1 of 559.87 Ω in Fig. 3 is used in order to control the current through the sample via measuring the potential difference V_1. The measured sample displacement versus time is illustrated in Fig. 4. There are three periods of sample movement as follows: (1) pre-movement time: the sample is still in place without any movements on the inclined plate after the DC power is activated; (2) acceleration: the sample is accelerated; and (3) constant movement: the sample moves at a constant speed. The sample average velocity (V_0) was determined at third period.

Fig. 3 Schematic view of the electro-tribometer

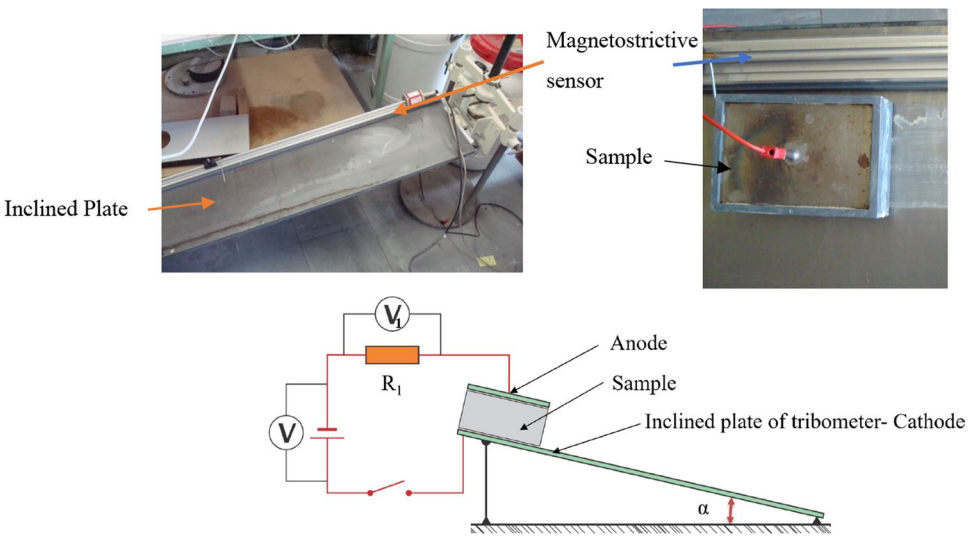

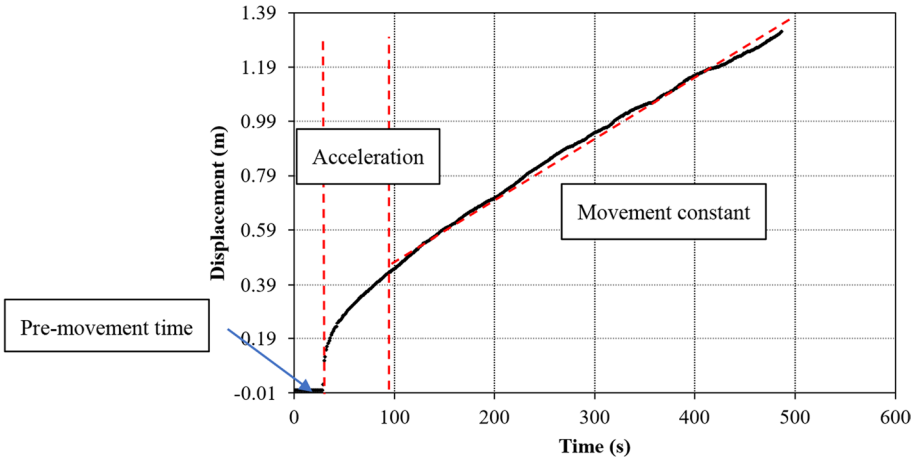

Fig. 4 Illustration of sample displacement measured versus time at 14° slope and 30 V of potential difference

At the end of each test, the sample surface, which was in contact with the metal plate, has been photographed (Fig. 5).

3.2 Characterization of sample movement

Figure 6 shows the influence of the potential difference on the pre-movement time (Fig. 6a) and the sample average velocity (V_0) (Fig. 6b). In all the tests, the application of the electric field does not instantly induce the movement of the samples. The increase of potential difference (ΔU) reduced the time necessary for the appearance of the movement (Pre-movement time). The tests carried out at $\Delta U = 5$ V, which is a limit to the exploitation of the phenomenon in the context of the study.

It can be seen in Fig. 6b that the sample velocity almost linearly increases with the increase in the potential difference except for the test result at $\Delta U = 5$ V. This can be attributed to the measurement errors or uncertainties due to stick–slip movement. Indeed, length movement is not large enough to analyze the exact velocity.

4 Lubrication phenomena

4.1 Hypothesis

The test duration is about 20 min. Thus, the hydration process of the cement-based material sample can be neglected and does not influence the rheological properties of the tested mixture. Because the sample velocity was almost constant during its total movement, the fluid film thickness can be assumed constant and is very thin compared to the sample dimensions. Under the effect of direct current (DC), the electro-osmosis phenomenon induces the water flow from the anode to the cathode, thus changing the rheological properties of the bottom layer of the sample via changing the solid volume fraction of the mixture.

Furthermore, from the observation of the sample's constant movement, the following hypotheses are assumed to determine the properties of the thin film fluid at the interface during the movement stage of the samples: (1) The sample is moved via a thin film fluid created by the electro-osmosis phenomenon. It is the region 1 as shown in Fig. 7. The solid volume fraction of this layer is smaller than that of the original mixture (Figs. 3, 5). (2) The rheological properties of the thin film are constants when the sample is moving.

4.2 Rheological properties of the mixtures

The rheological behavior of the cement-based material samples is identified by modifying the solid volume fraction in the mixture. The Malvern Gemini 150 rheometer (Fig. 8) is equipped with a plate–plate geometry (40 mm diameter) is used. The face of each plate is roughened to avoid slippage with the wall. The mixture behavior is studied in the coordinates $(\tau, \dot{\gamma}, \phi)$, where τ is the shear stress, $\dot{\gamma}$ is the shear velocity, and ϕ is the solid volume fraction. In this test setup, the distance between the two planes is kept constant at 2 mm.

Samples are prepared following a similar protocol to the paste preparation for the friction test. The fluid phase consisting of water and the plasticizer is prepared by remaining the ratio between the plasticizer dosage and the water dosage. The fluid mixture was mixed with the powder mixture for two minutes.

Before starting the rheological characterization test, the mixture age is noted and remains the same time for each test. The mixture is then placed in the cell plan-plan and the test starts with a pre-shear phase at 100 s^{-1} during 60 s, which ensures the mixture homogeneity. The characterization began with a restructuring linear phase down to = 0.1 s^{-1} for 100 s and a disintegration linear phase up to 100 s^{-1}

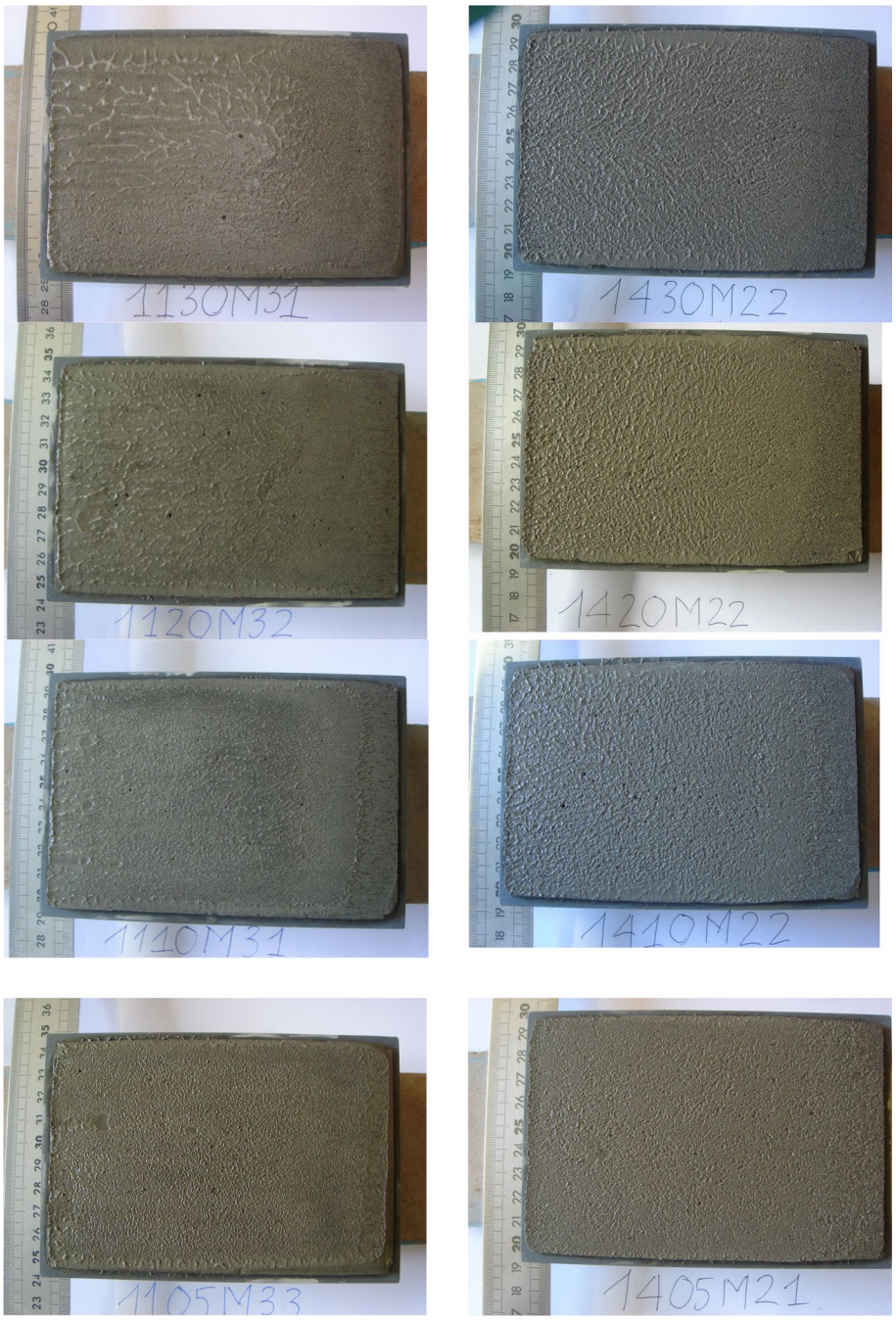

Fig. 5 Textures of the tested mortar samples at 5 V,10 V, 20 V, 30 V at 11° (left) and 14° (right)

(Fig. 9). During the test, shear strain and shear velocity are recorded. A flow curve illustration is obtained with different solid volume fractions as shown in Fig. 10. The parameters of the rheological properties are determined by matching the experimental data with the Herschel–Bulkley's flow curve that is given in Eq. (1):

$$\tau = \tau_0 + k.\dot{\gamma}^n, \tag{1}$$

where τ_0 is the limit yield stress, k is the flow parameter, and n is the structuring parameter. Each of these parameters depends on the solid volume fraction (ϕ).

As can be seen in Fig. 10 the limit yield stress exponentially increases as the shear velocity and the solid volume fraction increase.

The influence of $\dot{\gamma}$ on the limit yield stress τ_0 is shown in Fig. 11. These field data are obtained by a dynamic method consisting of the structuring phases and disintegration phases. A significant difference in the values of

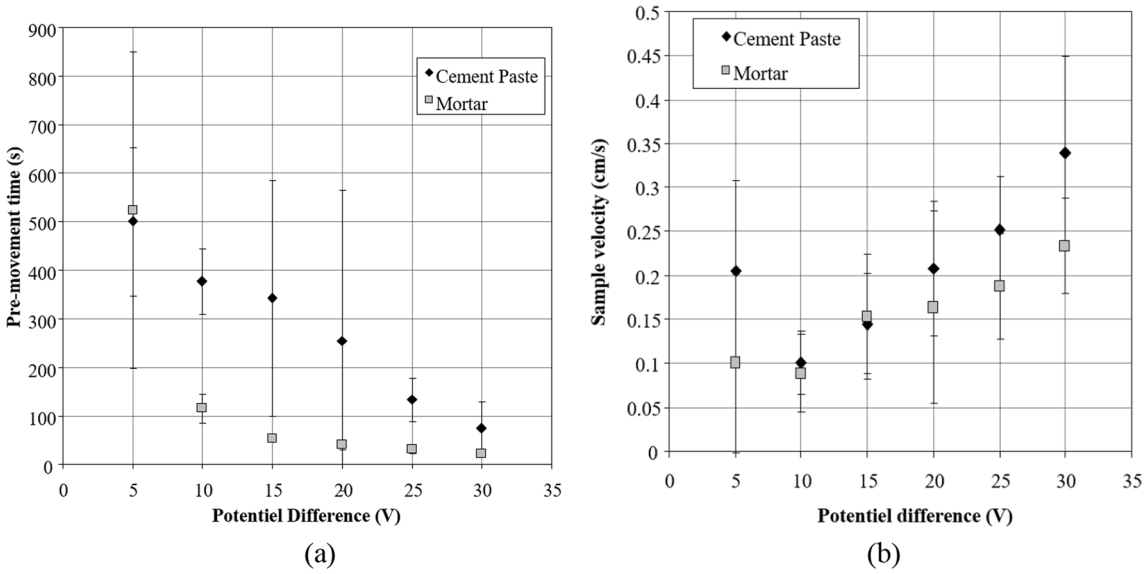

Fig. 6 Relationship of average evolution of **a** pre-movement time and **b** V_0 as a function of the potential difference (ΔU)

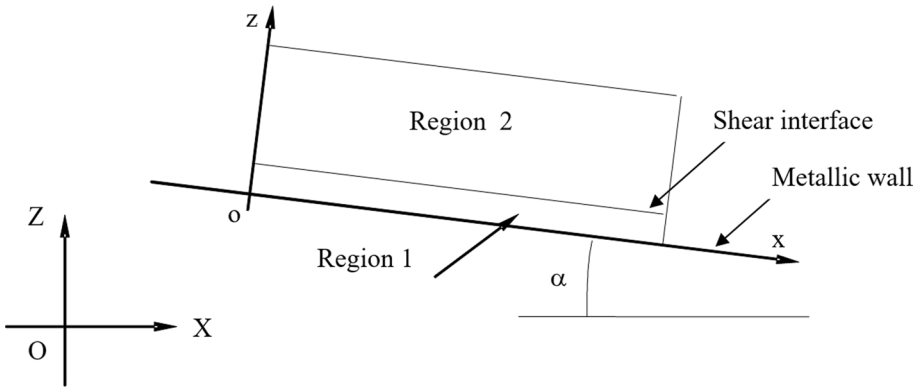

Fig. 7 Hypotheses of calculation

Fig. 8 Illustration of Rheometer Malvern Gemini 150

the limit yield stresses between the two phases has been found. The data parameters are modeled following the Le Grand's model expressed by Eq. (2):

$$\tau_0 = \tau_0^*.Exp(B(\phi - 0.5)), \tag{2}$$

where B,τ_0^* are constants.

The average structuring parameter in restructuring phases is determined to be $\overline{n} = 1.28$ for cement paste and $\overline{n} = 1.26$ for mortar (Fig. 12a) and is not influenced by the solid volume fraction. Some errors can be explained by the use of a small amount of materials for the mixture (about 30 g) and sample mixing was done manually. Sedimentation phenomena appeared in the case of cement paste at the lower solid volume fraction after mixing. This phenomenon affected the rheological

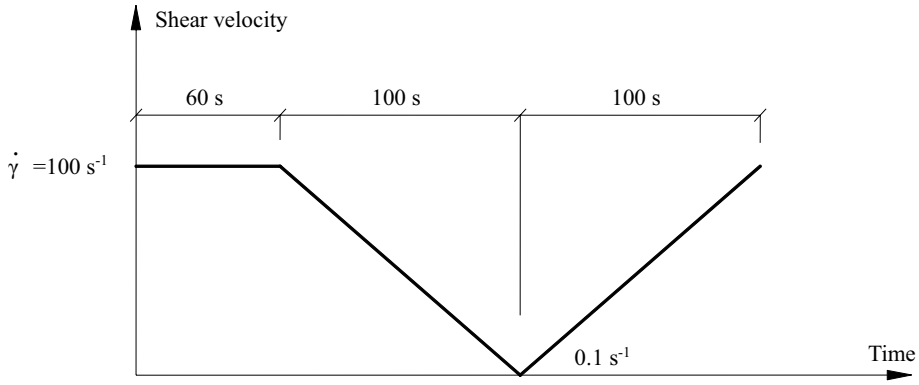

Fig. 9 Schematization of the rheological characterization protocol at imposed shear rate

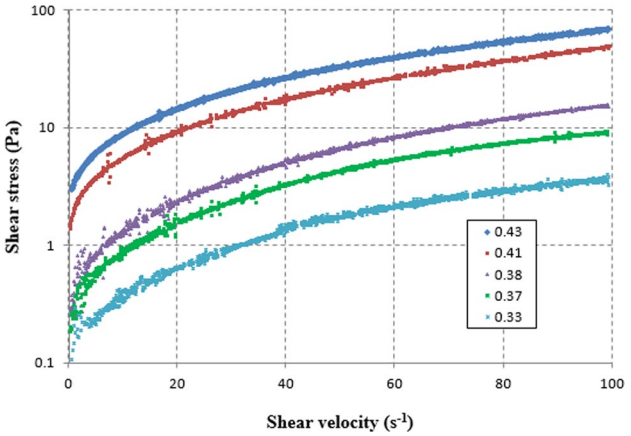

Fig. 10 Flow curves of cement paste $\tau=f(\dot{\gamma})$ for different values of solid volume fraction (ϕ)

results. Using the restructuring and disintegration phases, the rheological properties can be characterized as shown in Table 2.

The k parameter of the Herschel–Bulkley model is also analyzed. It represents the viscosity and is affected by the solid volume fraction as shown in Fig. 13.

It is noted that at a low value of ϕ, the k value tends to be asymptotic to the horizontal axis and is close to the water fluid viscosity. The k value goes asymptotically to the vertical axis at a higher value of ϕ. This is the limit solid volume fraction and is called the packing solid volume fraction (ϕ_M). The experimental data can be fit to the Krieger–Dougherty modified model as shown in Eq. (3):

$$k = k_0\left(1 - \frac{\varphi}{\varphi_M}\right)^{-\eta.\varphi_M}. \tag{3}$$

In this study, the parameters are computed using the least squares method with the Levenberg–Marquardt algorithm. The fitted parameters for Eq. (4) are given in Table 2.

$$\tau = \tau_0^*.Exp(B(\phi - 0.5)) + k_0(1 - \frac{\phi}{\phi_M})^{-\eta.\phi_M}\,\bar{\dot{\gamma}}^{\bar{n}}. \tag{4}$$

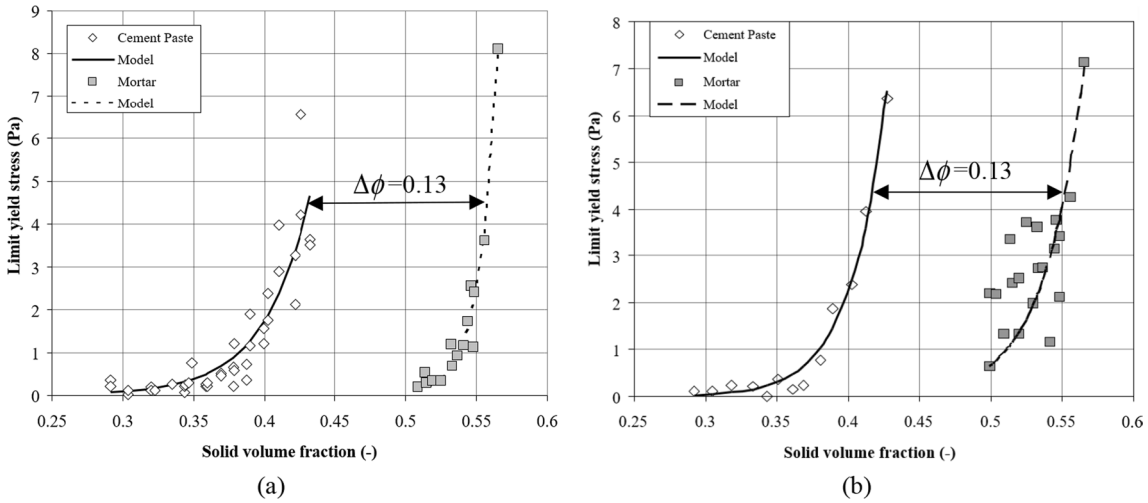

Fig. 11 Evolution of limit yield stress as a function of solid volume fraction in **a** restructuring phases and **b** disintegration phases

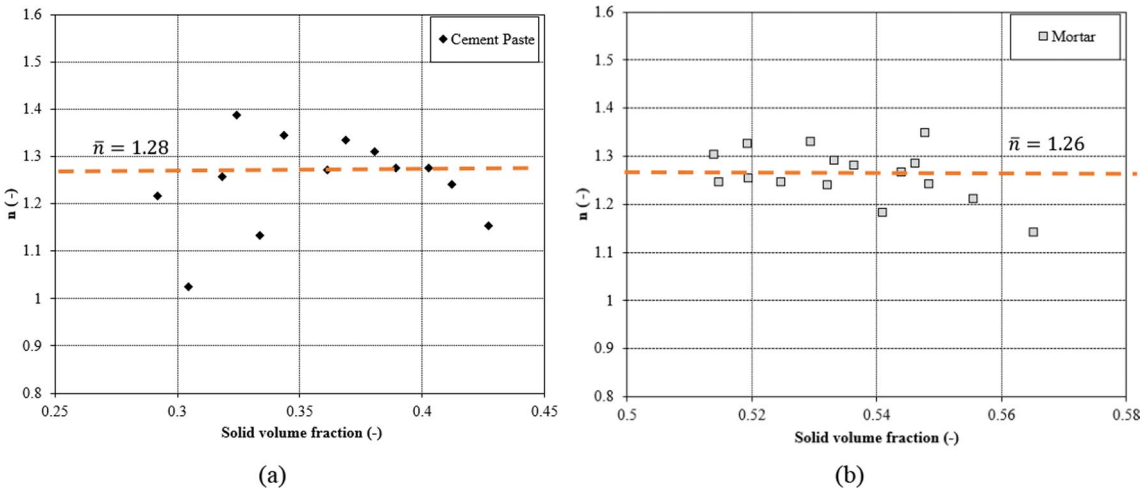

Fig. 12 The average structuring parameter in restructuring phases **a** cement paste and **b** mortar

Table 2 Rheological parameters of mixture

Phase	Type	τ_0^*(Pa)	B	k_0 (Pa.$s^{\bar{n}}$)	φ_M	η	$\bar{n}$
Restructuring	Cement paste	36.5	30.48	44×10^{-5}	0.46	5.48	1.28
	Mortar	5.19×10^{-2}	77.28	338×10^{-5}	0.59	2.45	1.26
Disintegration	Cement paste	117.24	39.65	6×10^{-4}	0.46	3.583	1.49
	Mortar	6×10^{-1}	36.3	8.9×10^{-4}	0.59	2.54	1.47

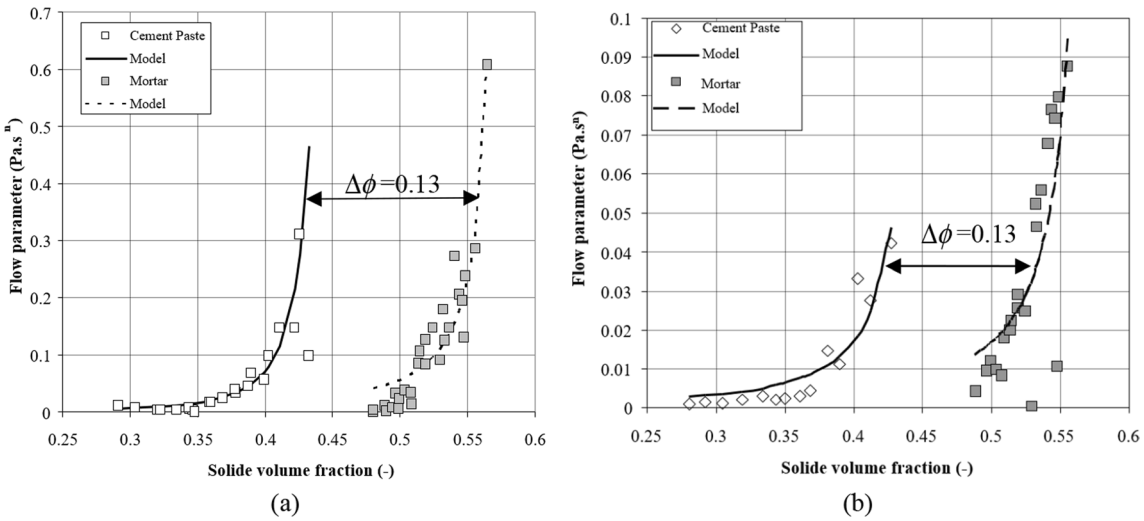

Fig. 13 Evolution of the Herschel–Bulkley model's k parameter as a function of solid volume fraction in **a** restructuring phases and **b** disintegration phases

Figures 11, 12, 13 show that the rheological behaviors of cement pastes and mortars are similar. Sand acts like an inclusion in the mortar and the rheological behavior of the mortar is controlled by the cement paste in the mortar. A gap $\Delta\phi = 0.13$ in the solid volume fraction between the two scales of materials is recorded. These results consistent with research of Toutou and Roussel [15]. The rheological model for cement pastes and mortars are used in the next section in order to calculate the solid volume fraction in the fluid film of test with electro-tribometer.

4.3 Equations

The equation describing the flux properties of the fluid film can be derived based on the mass conservation and the momentum conservation equation. The mixture is characterized by the solid volume fraction and this fraction is assumed to be constant during the test. The average volume mass is calculated using Eq. (5). In this model, the longitudinal pressure gradient is neglected.

$$\rho_{avg} = f.\rho_s + (1 - f)\rho_e, \tag{5}$$

where ρ_{avg}, ρ_s, and ρ_e are average volume mass, solid volume mass, and fluid volume mass, respectively.

The boundary conditions are as follows: (1) a constant pressure induced by the sample weight acting on the film, (2) the perfect bond between the film and the wall, and (3) the shear stress at the depth of $z = h$ constantly induced by the sample weight (Fig. 7).

Finally, given the rheological behavior law of a non-Newtonian fluid, the film fluid properties are determined by the average solid volume fraction using Eqs. (6, 7):

$$V_0 = \frac{k_0\left(1 - \frac{\phi}{\phi_M}\right)^{-[\eta]\phi_M}}{\left[\frac{2}{L}\frac{Mg\cos\alpha}{S} - \left[\phi.\rho_s + (1-\phi)\rho_e\right].g.\sin\alpha\right].(\frac{1}{n}+1)}.\left[\left(\frac{\frac{Mg\sin\alpha}{S} - \tau_0^*.e^{A.(\phi-0.5)}}{k_0\left(1 - \frac{\phi}{\phi_M}\right)^{-[\eta]\phi_M}}\right)^{\frac{1}{n}+1} - \left(\frac{C}{k_0\left(1 - \frac{\phi}{\phi_M}\right)^{-[\eta]\phi_M}}\right)^{\frac{1}{n}+1}\right], \tag{6}$$

$$C = \frac{Mg\sin\alpha - F_{fr}}{S} - \tau_0^*.e^{A.(\phi-0.5)} - \frac{2}{L}\frac{Mg\cos\alpha}{S}\frac{\Delta M}{\left[\phi.\rho_s + (1-\phi)\rho_e\right].l.L_T} + .g.\frac{\Delta M}{l.L_T}\sin\alpha, \tag{7}$$

where C is a variable of Eq. (6) to reduce the length of Eq. (6) and

$$\Delta M = \left[\rho_s\phi + (1-\phi)\rho_e\right]h.l.L_T, \tag{8}$$

In Eqs. (6 and 7), the solid volume fraction is the unique variable. If the mixture flow volume is assumed to be a constant (which is compatible with the sample velocity), the average film height will be given by the following condition:

$$h = \frac{\Delta M}{\rho_{avg}.l.L_T}, \tag{9}$$

where M is the initial sample mass, ΔM is the sample mass loss, α is the wall inclination angle, V_0 is the sample velocity, S is the sample surface area in contact with the wall, l is the sample width, and L_T is the displacement length of sample in inclined plate.

5 Results and discussion

5.1 (1) Characterization of rheological properties of interface film

Samples of the same mixture are tested with different slope angles and potential differences. For each tested sample, the average solid volume fraction and the average film height of interface film were determined by Eqs. (6, 7, and 8). Figure 14 shows the plots of the relationship between the potential difference and the average solid volume fraction of this film. It can be noted that there always be a unique solution with a packing volume fraction. Moreover, the results show that the potential difference affects the modification of the mixture texture in contact with the wall. The results show that the shear stress is generally constant, which is resulted from the average film thickness of $h = 1.29 \times 10^{-5}$ m (Fig. 15).

5.2 (2) Characterization of rheological properties of interface film

In this study, the flow of electro-osmotic is determined using the mass conservation as shown in Fig. 16. The electro-osmotic flow is equal to the flow of lubrication or mass deposition on the inclined plate. The effect of potential difference on the electro-osmotic permeability coefficient has been assessed. This coefficient is calculated using the following formula based on the Casagrande's law:

$$Q_{Lubrification} = Q_{electro-osmotic}, \tag{10}$$

$$Q_{electroosmotic} = \frac{\Delta M.V_0}{\left[\rho_s.\varphi + (1-\varphi)\rho_e\right]hlL_T} = k_{eq}S\frac{\Delta U}{H}, \tag{11}$$

where ΔM is the mass losses (g); V_0 is the sample velocity (m/s); ΔU is the potential difference; H is the sample thickness (m); S is the sample area (m^2); k_{eq} is the electro-osmotic

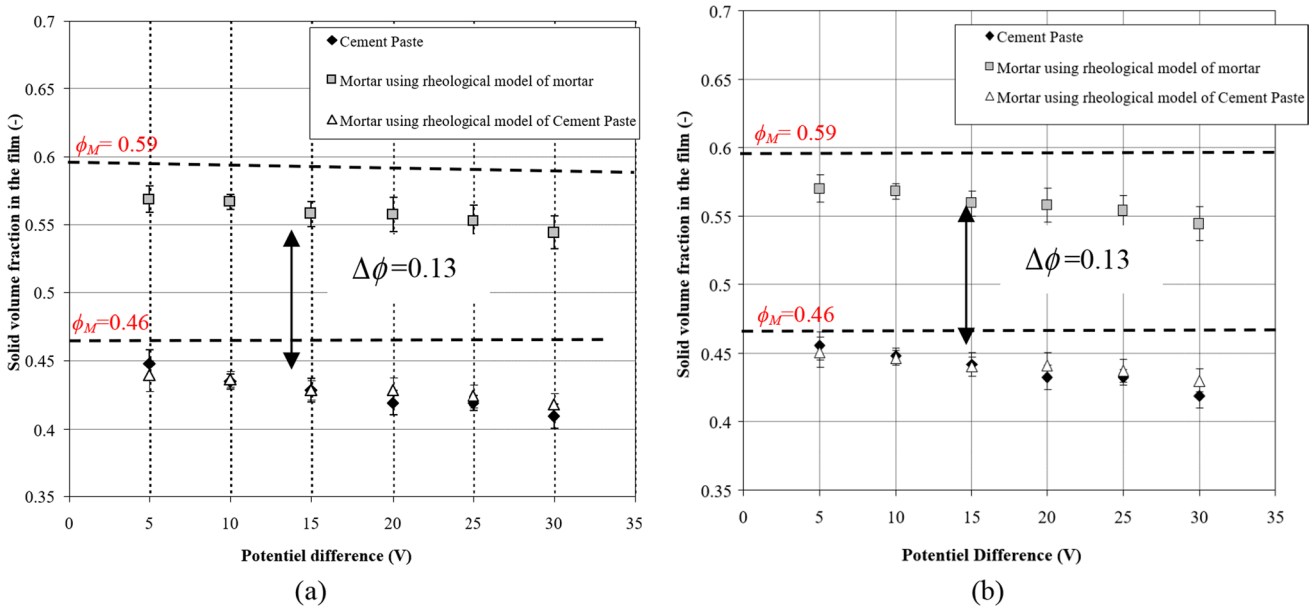

Fig. 14 Evolution of solid volume fraction as a function of the electrical potential difference with cement paste and mortar material in **a** restructuring phases and **b** disintegration phases

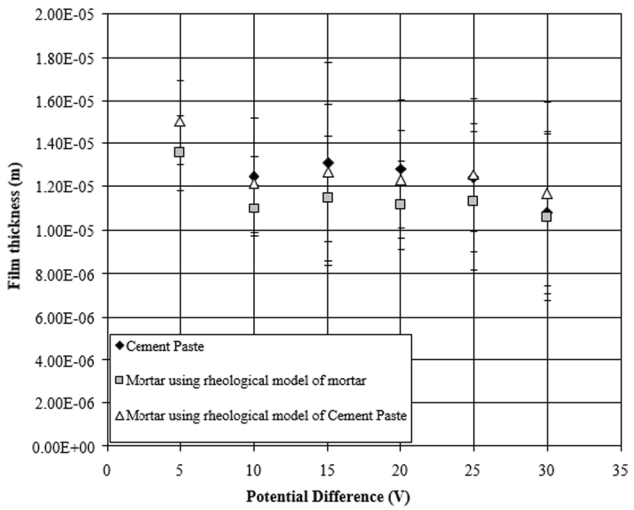

Fig. 15 Evolution of the height of fluid film (h) as a function of the potential difference (ΔU)

permeability coefficient; l is the sample width (m); and L_T is the displacement length of sample in inclined plate (m).

In Eq. (10), all parameters are determined after each test. The results are reported in Fig. 17 by establishing the relationship between the potential difference and the flow of electro-osmotic. Two scales of material are analyzed.

Figure 17 shows the linear relationship between the electro-osmotic flow and $Q_{electro\text{-}osmotic}$. These results permit the identification of an electro-osmotic permeability coefficient with good confidence. Indeed, the results of electro-osmotic permeability are $k_{cement\ paste} = 3 \times 10^{-10}$ m^2.V^{-1}.s^{-1} ($R^2 = 90\%$) for cement pastes and $k_{mortar} = 2 \times 10^{-10}$ m^2.V^{-1}.s^{-1} ($R^2 = 91\%$) for mortars. These values remain lower than those in the literature [11]. These low values can be attributed to the use of small amount of water in the extrudable mixtures compared to cast-in-place cement-based materials (cast-in-place concrete).

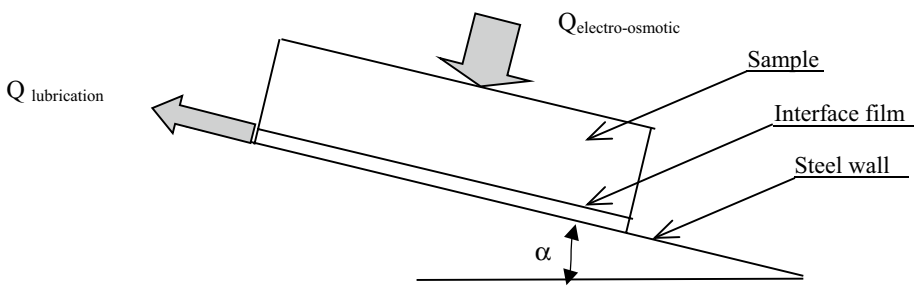

Fig. 16 Schematic of flow coupling: electro-osmotic and lubrication

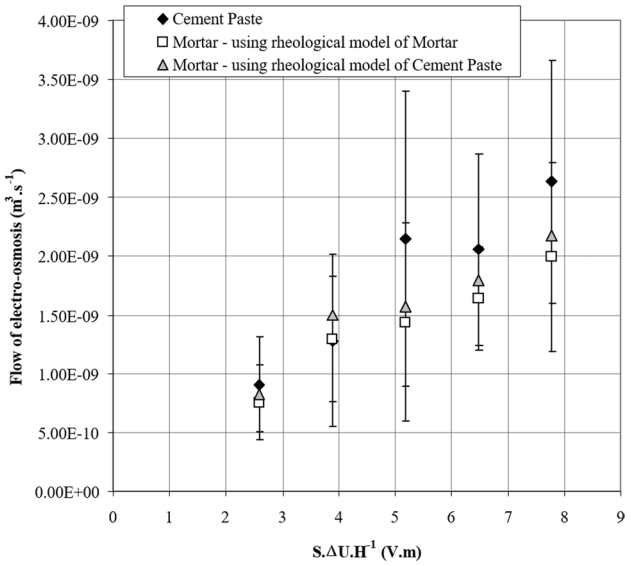

Fig. 17 Lubrication control study between fluid mass flow and electrical potential difference

6 Conclusions

This study has investigated the effect of electro-osmosis on lubricating the interface between the extrudable cement-based material samples and metal plate. The electro-tribometer was used in this study. The two-scale material was used for testing. The displacement development was measured using a magnetostrictive sensor. Some of the important findings from this study are summarized as follows:

(1) The principle of electro-osmosis via using a direct current (DC) has great effect on modification of rheological properties of cement-based materials in contact with a metal plate.
(2) The effect of lubrication on the interface cement-based material samples and the metal plate is observed in a developed electro-tribometer. Under the effect of sample weight posed on the inclined plane, no movements have been recorded until the application of potential difference between the two areas of the sample. Three periods consisting of pre-movement time, acceleration, and movement stability are observed during all of the tests. The stick–slip shape of displacement appears at 5 V of potential difference.
(3) Logically, when the potential difference increases from 10 to 30 V, the pre-movement time decreases and the velocity of the sample increases.
(4) Assuming that the sample velocity is constant with time, a thin film fluid appears in the interface between the cement-based material sample and the metal plate with a constant height. An equation has been established between the solid volume fraction and the tested data. The average film thickness of $h = 2.29 \times 10^{-5}$ m has been determined and it can clarify the influence of potential difference on the solid volume fraction of the lubricating film fluid.
(5) From the experimental data, the electro-osmotic permeability coefficient can be indirectly calculated. These values remain lower than those in the literature. This can be attributed to the use of small amount of water content in the mixture.

Limitations of this study is not examined of the consolidation effect of mixture during extrusion process that can be induced the movement of fluid and changed the solid volume fraction in the mixture. This test is compatible with firm cement-based materials used in extrusion process. For future work, the effect of electro-osmosis on the mechanical properties of cement-based materials should be experimentally conducted.

Author contributions Viet Hai Hoang contributed to writing, testing, and editing, investigation, and data curation. Yannick Mélinge was involved in conceptualization, methodology, and data curation. Christophe Lanos performed methodology, visualization and editing. Anh Tu Do and Anh Tuan Tran were involved in writing—reviewing and editing.

Declarations

Conflict of interest The authors declare that they have no known competing financial interests or personal relationships that could have appeared to influence the work reported in this paper.

References

1. Perrot A et al (2006) Ram extrusion force for a frictional plastic material: model prediction and application to cement paste 45:457–467. https://doi.org/10.1007/s00397-005-0074-y
2. Perrot A et al (2007) Mortar physical properties evolution in extrusion flow. Rheol Acta 46:1065–1073. https://doi.org/10.1007/s00397-007-0195-6
3. Perrot A et al (2019) Extrusion of cement-based materials: an overview. RILEM Tech Lett 3:91–97. https://doi.org/10.21809/rilemtechlett.2018.75
4. Winkel A (2014) Reduction of extrusion wall friction in a screw press by electroosmosis, part 1. Interceram - Int Ceram Rev 63(4):202–206. https://doi.org/10.1007/BF03401059
5. Mélinge Y et al (2013) Study of tribological behaviour of fresh mortar against a rigid plane wall. Eur J Environ Civ Eng 17(6):419–429. https://doi.org/10.1080/19648189.2013.786242
6. Toutou Z, Roussel N, Lanos C (2005) The squeezing test: a tool to identify firm cement-based material's rheological behaviour and evaluate their extrusion ability. Cem Concr Res 35(10):1891–1899. https://doi.org/10.1016/j.cemconres.2004.09.007

7. Djelal C (2001) Designing and perfecting a tribometer for the study of friction of a concentrated clay-water mixture against a metallic surface. Mater Struct 34(1):51–58. https://doi.org/10.1007/BF02482200
8. Goudjil N et al (2014) Impact of temperature on the demoulding of concrete elements with a polarization process. Constr Build Mater 54:402–412. https://doi.org/10.1016/j.conbuildmat.2013.12.034
9. Goudjil N et al (2012) Electro-osmosis applied for formwork removal of concrete. J Adv Concr Technol 10(9):301–312. https://doi.org/10.3151/jact.10.301
10. Vanhove Y, Djelal C (2021) Influence of the formwork removal by polarization on the facing aesthetics in reinforced concrete. Constr Build Mater 284:122841. https://doi.org/10.1016/j.conbuildmat.2021.122841
11. Casagrande IL (1949) Electro-Osmosis in Soils 1(3):159–177. https://doi.org/10.1680/geot.1949.1.3.159
12. Mitchell JP (1976) Fundamentals of soil behaviour. Wiley, New York, USA
13. Cambefort H, Caron C (1961) Electro-Osmose et Consolidation Electro-Chimique des Argiles 11(3):203–223. https://doi.org/10.1680/geot.1961.11.3.203
14. Hoang VH (2011) Interaction fluide-structure: Comportement tribologique des matériaux minéraux à base cimentaire à l'état frais. Thesis (PhD) in INSA Rennes, France
15. Toutou Z, Roussel N (2006) Multi scale experimental study of concrete rheology: from water scale to gravel scale. Mater Struct 39(2):189–199. https://doi.org/10.1617/s11527-005-9047-y